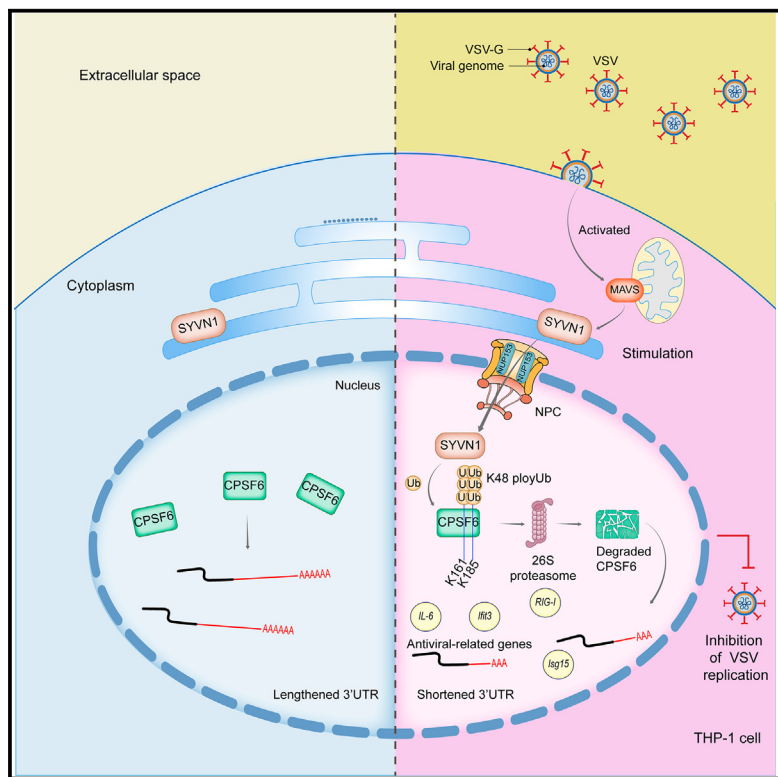


E3 ligase SYVN1-mediated polyubiquitination of CPSF6 promotes alternative polyadenylation and antivirus effects of macrophages

Graphical abstract



Authors

Xin Lu, Chao Liu, Runze Wu, ...,
Shangwu Chen, Yonggui Fu, Anlong Xu

Correspondence

fuyg@mail.sysu.edu.cn (Y.F.),
lssxal@mail.sysu.edu.cn (A.X.)

In brief

Lu et al. show the mechanism of APA regulation in macrophages upon VSV infection. MAVS activates the nuclear import of SYVN1, and then SYVN1 catalyzes the ubiquitination of CPSF6, resulting in CPSF6 degradation, APA switching, and antiviral effects. They identify the APA regulation mechanism in antiviral immune responses.

Highlights

- Protein, but not mRNA level, of CPSF6 is reduced in macrophages upon virus infection
- Reduced CPSF6 in macrophage promotes APA switching and antivirus effects
- E3 ligase SYVN1 catalyzes K48-linked polyubiquitination at K161/K185 residues of CPSF6
- MAVS triggers the nuclear import of SYVN1 upon viral infection



Article

E3 ligase SYVN1-mediated polyubiquitination of CPSF6 promotes alternative polyadenylation and antivirus effects of macrophages

Xin Lu,^{1,3} Chao Liu,^{1,3} Runze Wu,¹ Zhijie Hu,¹ Susu Liu,¹ Xuening Li,¹ Yuchi Liu,¹ Mengxia Li,¹ Jingting Liang,¹ Yingye Huang,¹ Yuting Han,¹ Xin Ou,¹ Ke Deng,¹ Cheng Liang,¹ Shangwu Chen,¹ Yonggui Fu,^{1,*} and Anlong Xu^{1,2,4,*}

¹State Key Laboratory for Biocontrol, Guangdong Province Key Laboratory of Pharmaceutical Functional Genes, Department of Biochemistry, Innovation Center for Evolutionary Synthetic Biology, School of Life Sciences, Sun Yat-sen University, Guangzhou 510275, China

²Sun Yat-sen University Institute of Advanced Studies, Hong Kong SAR 999077, China

³These authors contributed equally

⁴Lead contact

*Correspondence: fuyg@mail.sysu.edu.cn (Y.F.), lssxal@mail.sysu.edu.cn (A.X.)

<https://doi.org/10.1016/j.celrep.2025.115276>

SUMMARY

Transcriptome-wide alternative polyadenylation (APA) is involved in both innate and adaptive immune responses of immune cells. Downregulation of the CPSF6 protein, one of the 3' end-processing factors, mediates APA in macrophages with responses to virus infection and plays an important role in its anti-virus effect. However, the signaling pathway and molecular mechanism underlying the downregulation of the CPSF6 protein remain elusive. Here, we found that MAVS triggers the nuclear import of the E3 ligase SYVN1 mediated by NUP153 in response to vesicular stomatitis virus infection. Then, SYVN1 catalyzes K48-linked polyubiquitination of CPSF6, resulting in degradation of CPSF6 via the proteasome and then transcriptome-wide APA and anti-virus effects. Our results identify an antiviral mechanism via APA regulation based on ubiquitination modification of the CPSF6 protein, which may serve as a target for developing immune interventions.

INTRODUCTION

Pattern recognition receptors (PRRs) initiate the innate immune responses to viral infection.^{1,2} Extensive studies have been performed to illustrate the signaling pathways of PRRs. Among PRRs, RIG-I-like receptors (RLRs) play an important role in RNA virus recognition. After sensing and recognizing virus RNA, RLRs activate the adapter molecule MAVS, located on the mitochondrion outer membrane, which then triggers a signaling cascade for the production of type I interferon and proinflammatory cytokines and inhibits viral infection.³

Recently, alternative polyadenylation (APA), as a new way of gene expression network regulation, has attracted much attention in the field of immune responses, development, tumorigenesis, and so on with the development of genome-wide analytical methods.^{4–6} APA can generate mRNA isoforms with alternative 3' ends in eukaryotic cells by recognizing the different poly(A) signals on pre-mRNA and has a broad and profound impact on the complexity of the transcriptome. It has been found that immune cells activated by antigens or pathogens, such as T cells,^{7,8} macrophages,⁹ and zebrafish spleen tissues,¹⁰ display shorter 3' UTRs due to APA. Genes with APA switching in response to vesicular stomatitis virus (VSV) infection in macrophages are mainly enriched in immune-related categories such

as Toll-like receptor, RLR, JAK-STAT and apoptosis-related pathways,⁹ and the shortened 3' UTR of immune related genes can improve their mRNA stability and enhance translational efficiency, thereby promoting antiviral immune responses through type I interferon (IFN-I) signaling.¹¹ To better understand the effects of global APA switching in immune responses and to develop new immune intervention methods based on APA, we need to clarify the regulation mechanism of APA in immune responses.

Transcriptome-wide APA is usually regulated by altering the expression levels of core 3' end-processing factors and RNA binding proteins in immune cells and tumors.¹² 3' end-processing machinery consists of more than 20 core proteins, including four protein complexes (cleavage factor I mammalian [CFIm], CFIIIm, cleavage and polyadenylation specificity factor [CPSF], and cleavage simulation factor [CstF]) and several individual proteins that perform pre-mRNA cleavage and polyadenylation by recognizing *cis* factors.⁵ During B cell differentiation, elevated expression of CstF64 promotes a switch to the proximal poly(A) site of the immunoglobulin μ heavy-chain gene, resulting in the production of an immunoglobulin M (IgM) isoform that lacks the transmembrane domain, allowing the antibody to be secreted.^{13,14} The elevated expression of CstF64 has also been found in T cells upon T cell receptor activation, which leads to the preferred



proximal poly(A) site of the transcription factor NF-ATc, which promotes the expression of interleukin-2 (IL-2).¹⁵ We also found elevated expression of SNRPA during T cell differentiation, which promotes the usage of proximal poly(A) sites of STAT5b.⁸ The CFI complex, composed of CPSF5 and CPSF6, plays an important role in regulating APA.^{16,17} Losing CFI function leads to preferred usage of proximal poly(A) sites, resulting in transcriptome-wide shorter 3' UTRs.¹⁸⁻²¹ Our team has recently found downregulation of CPSF6 protein in macrophages with viral infection, resulting in a globally shortened 3' UTR,¹¹ but the molecular mechanism of the dramatic decrease of CPSF6 protein still remains unknown.

Here, we found that MAVS mediates the re-localization of the E3 ligase SYVN1 to the nucleus in macrophages upon VSV infection. Then, SYVN1 interacts with CPSF6 and degrades it via the ubiquitinated proteasome pathway, resulting in globally shorter 3' UTRs at the transcriptome-wide level, which promotes anti-viral immunity.

RESULTS

Remarkable protein but not mRNA reduction of CPSF6 along with globally shortened 3' UTRs in macrophages after VSV infection

Here, with 3' end sequencing using the IVT-SAPAS method,^{22,23} we confirmed the globally shortened 3' UTR in a human monocytic leukemia (THP-1) cell line with infection of VSV (an RNA virus) (Figure 1A; Table S1). The data also show no significant mRNA expression changes of the core 3' end-processing factors with the known effects of promoting or repressing proximal poly(A) sites (Figure 1B). We then examined protein levels of CPSF5, CPSF6, and CPSF7 in THP-1 cells and found that only the protein level of CPSF6 is significantly reduced following VSV infection (Figures 1C, S1A, and S1B). Furthermore, the reduction in protein but not mRNA level of CPSF6 was also observed in primary peritoneally derived macrophages (PMs) (Figure 1D) and bone marrow-derived macrophages (BMDMs) (Figure 1E) of C57BL/6J mice and mouse L929 cells (Figure S1C) after VSV infection. Subsequently, we treated THP-1 cells with poly(I:C) (Low molecular weight, LMW), poly(dA:dT) (Figures 1F and 1G), herpes simplex virus type 1 (HSV-1; a DNA virus) (Figure S1D), and Sendai virus (an RNA virus) (Figure S1E), and CPSF6 expression also showed a similar albeit weaker pattern. This reveals that the reduction of CPSF6 protein in macrophages responding to viral infection is not regulated by a mRNA transcriptional process, indicating that an alternative regulatory approach may be post-translational modification and degradation.

Degradation of CPSF6 protein through the ubiquitin-proteasome pathway by the E3 ligase SYVN1

Post-translational modifications can regulate protein abundance to regulate biological functions. Primary intracellular protein degradation systems include ubiquitin-proteasome and lysosomal pathways.^{24,25} In order to ascertain the potential pathway responsible for the degradation of CPSF6, we treated THP-1 cells with the proteasome inhibitor carboxybenzyl-L-leucyl-L-leucyl-L-leucine (MG132)²⁶ and the autophagy inhibitors of 3-methyladenine (3-MA) and baflomycin A1 (Baf-A1)²⁷ and

again measured the protein abundance changes of CPSF6 upon VSV infection. The results show that MG132 can block VSV-mediated CPSF6 degradation in THP-1 (Figure 2A). In contrast, 3-MA and Baf-A1 cannot inhibit CPSF6 protein degradation following viral infection (Figures S2A and S2B). Furthermore, immunoprecipitation of CPSF6 was performed for the cells with MG132 treatment and VSV infection, and western blot with anti-Ubiquitin (anti-Ub) showed a higher ubiquitination level of CPSF6 in the cells with MG132 treatment than DMSO (Figure 2B). These results suggest that the reduction of CPSF6 protein after VSV treatment is mediated by ubiquitination modification and subsequent degradation through the ubiquitin-proteasome pathway.

The ubiquitin-proteasome pathway functions with an enzymatic cascade, which includes three groups of enzymes termed ubiquitin E1 (activating enzyme), ubiquitin E2 (conjugating enzyme), and ubiquitin E3 (ligase), and the key enzyme that specifically catalyzes ubiquitination of the target protein is the Ub-E3 protein ligase.^{28,29} With UbiBrowser 2.0 (<http://ubibrowser.bio-it.cn/>), we found seven potential E3 ligases for CPSF6 (Figure S2C). To identify the E3 ligase for CPSF6, we knocked down the potential E3 ligases with small interfering RNA (siRNA) in THP-1 cells and then measured the ubiquitination modification level of CPSF6 after viral infection with anti-Ub following immunoprecipitation of CPSF6. The results show that knockdown of SYVN1 leads to significantly reduced ubiquitination and an elevated expression level of CPSF6 protein (Figures S2D and S2E). We further examined the effect of SYVN1 on changes of ubiquitination and expression levels of CPSF6 in THP-1 cells upon VSV infection. Whereas VSV infection leads to significantly elevated ubiquitination and reduced expression levels of CPSF6 in control cells, as expected, SYVN1 knockdown can inhibit the protein degradation of CPSF6 and repress ubiquitination modification of the CPSF6 protein triggered by viral infection (Figure 2C). The small molecule LS-102 has a selective inhibitory effect on SYVN1 enzymatic activity.³⁰ Treatment of THP-1 with LS-102 also shows a significant lower level of ubiquitination modification of CPSF6 than the control in response to VSV infection (Figure 2D). Furthermore, double knockdown of SYVN1 and MG132 treatment of SYVN1 reveals that the effect of MG132 treatment is less in cells with SYVN1 knockdown than in control cells, suggesting that SYVN1 mediates the degradation of CPSF6 through the ubiquitinated proteasome pathway upon VSV infection (Figure S2F). All of this suggests that the E3 ligase of SYVN1 may mediate the ubiquitination modification and degradation of CPSF6 protein during VSV infection and play an important role in 3' UTR shortening and antiviral innate immunity.

SYVN1 directly interacts with CPSF6

To further confirm the effect of SYVN1 on ubiquitin-mediated degradation of CPSF6, we investigated whether SYVN1 can interact with CPSF6 directly. With antibodies against CPSF6 and SYVN1, a co-immunoprecipitation colIP assay shows that endogenous CPSF6 and SYVN1 can pull down each other in THP-1 cells with the treatment of MG132 and VSV infection (Figures 3A and 3B). We co-expressed Myc-CPSF6 and FLAG-SYVN1 in HEK293T cells and performed colIP with anti-Myc and

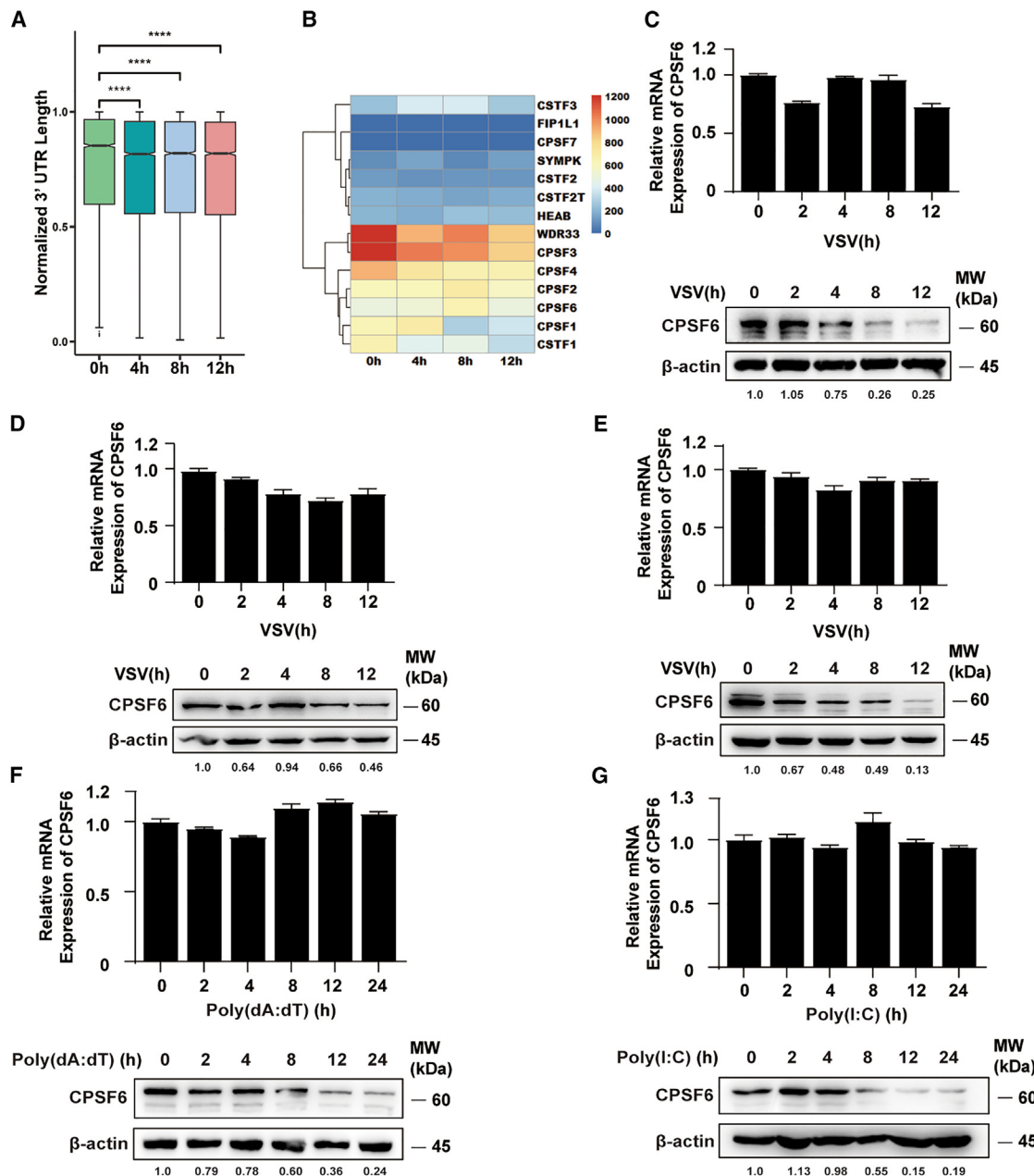


Figure 1. Downregulated CPSF6 protein in macrophages upon viral infection

(A) Notched boxplot of weighted mean 3' UTR length of THP-1 cells upon VSV (MOI = 1) infection at 0, 4, 8 and 12 h. ****p < 0.0001 with paired t test. Two biological repeats were performed with IVT-SAPAS.

(B) Heatmap of mRNA expression levels of 3' end-processing factors.

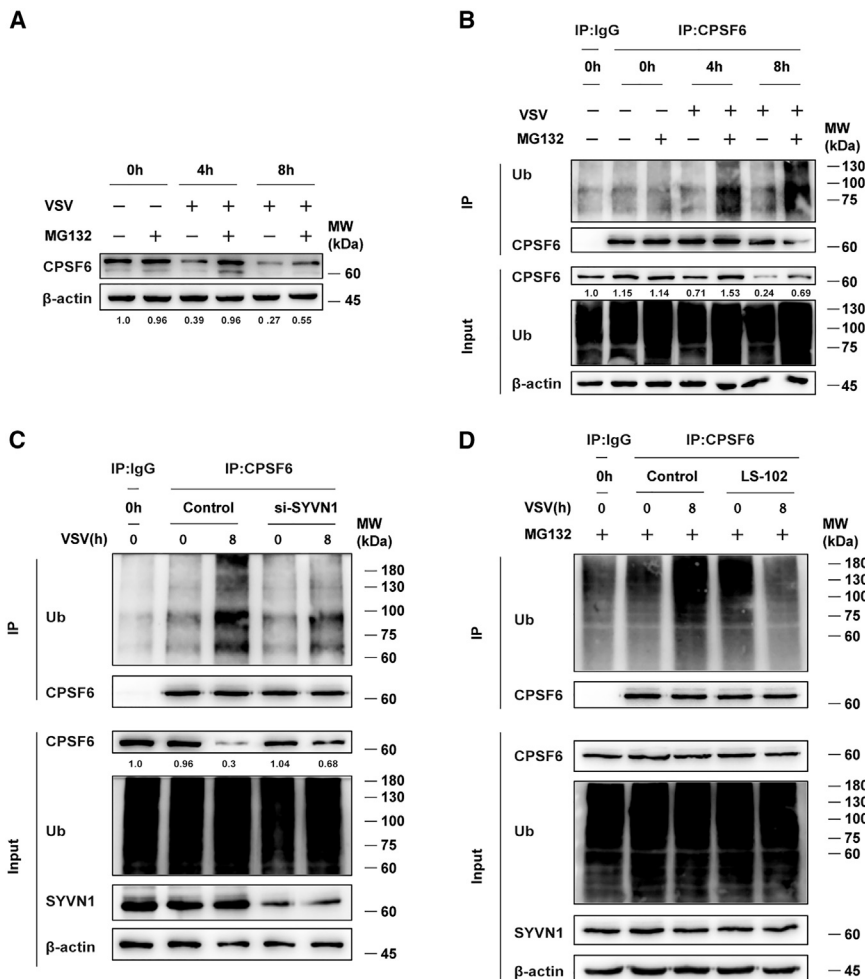
(C) Western blot and RT-qPCR analysis of CPSF6 protein and mRNA levels in THP-1 cells upon VSV (MOI = 1) infection at the indicated time points. β-actin was used as a loading control. Error bars indicate SD ($n = 3$ replicates).

(D and E) Protein and mRNA expression levels of CPSF6 in C57BL/6 mouse PMs and BMDMs infected with VSV at different time points. Error bars indicate SD ($n = 3$ replicates).

(F and G) Protein and mRNA expression levels of CPSF6 in THP-1 cells stimulated with poly(dA:dT) and poly(I:C). All RT-qPCR experiments were performed with three biological replicates, and β-actin was used as an internal control. Error bars indicate SD ($n = 3$ replicates).

anti-FLAG, respectively, and the results also show that there is robust interaction between them (Figures 3C and 3D). Furthermore, CPSF6 can pull down more SYVN1 with increasing duration

of virus infection and reaches the highest level at 8 h of viral infection (Figure 3E). To identify the domain of CPSF6 that can interact with SYVN1, we split CPSF6 into three segments (N terminus and



RNA recognition motif [RRM], proline-rich domain [PRD], and arginine/serine-like domain [RSLD]) and fused a Myc tag at their N termini (Figure 3F). We then co-expressed them with FLAG-SYVN1, and coIP with anti-Myc showed that only the RRM domain of CPSF6 could pull down FLAG-SYVN1 as the full length of CPSF6 does (Figure 3G). These results demonstrate that SYVN1 can interact with CPSF6 directly.

SYVN1 targets K161/K185 of CPSF6 for K48-linked polyubiquitination

The function of polyubiquitination modification is determined by the type of ubiquitin linkage.²⁹ To investigate the ubiquitin linkage type of CPSF6 ubiquitination, we obtained seven ubiquitin mutants with single lysine only (Figure 4A) and co-expressed the hemagglutinin (HA)-ubiquitin mutants, Myc-CPSF6, and FLAG-SYVN1 in the HEK293T cell line and infected the cells with VSV. A coIP assay showed that CPSF6 could be ubiquitinated by K11, K27, K48, and K63 ubiquitins (Figure 4B). We then overexpressed these HA-ubiquitin mutants and treated the cells with MG132 and VSV. CoIP with anti-CPSF6 showed that K48- and K63-linked ubiquitin could enhance the ubiquitination level of endogenous CPSF6 in cells with MG132 treatment

Figure 2. CPSF6 is degraded through the ubiquitination-proteasome pathway by the E3 ligase SYVN1

(A) Western blot analysis of CPSF6 protein expression in THP-1 cells with treatment of MG132 (10 μM) or DMSO. The cells were infected with VSV-EGFP (MOI = 1) for 4 and 8 h before sample collection.

(B) Elevated ubiquitination level of CPSF6 upon VSV infection. THP-1 cells were treated with MG132 or DMSO and then infected with VSV-EGFP for 4 and 8 h, followed by IP with anti-CPSF6 and western blot with anti-Ub and anti-CPSF6.

(C) Knockdown of SYVN1 attenuates the ubiquitination of CPSF6 upon VSV infection. THP-1 cells were transfected with SYVN1 siRNA for 48 h and infected with VSV-EGFP for 8 h ($n = 3$ replicates).

(D) The SYVN1 inhibitor represses the ubiquitination of CPSF6. THP-1 cells were treated with SYVN1 inhibitor LS-102 (10 μM) and MG132 for 8 h and infected with VSV-EGFP for 8 h, followed by IP with anti-CPSF6 and western blot with anti-Ub and anti-CPSF6. Homologous IgG was used as a negative control.

compared to the control cells, as the wild-type ubiquitin does (Figure 4C). In the cells with overexpression of the wild type of ubiquitin, with antibodies specific to K48- and K63-linked ubiquitin chains, we found that SYVN1 can increase K48-linked ubiquitination of CPSF6 but not K63 (Figure 4D). This observation indicates that K48-linked ubiquitination plays a role in mediating CPSF6 degra-

dation, which is consistent with its established role in regulating protein degradation.³¹ It has been found that C329S mutation of SYVN1 can inactivate its E3 ligase activity.³² We co-expressed FLAG-SYVN1-WT or the mutant FLAG-SYVN1-C329S (Figure 4A) with HA-K48 ubiquitin and Myc-CPSF6 in HEK293T cells, and the result showed that the C329S mutant could significantly decrease K48-linked ubiquitination of CPSF6 compared to the wild-type SYVN1 (Figure 4E). These findings collectively reveal that SYVN1 plays a role in mediating K48-linked ubiquitination of CPSF6.

Three lysine residues (K79, K161, and K185) of CPSF6 are predicted to be the potential ubiquitination sites by SYVN1 with UbiBrowser 2.0. To determine the polyubiquitination sites of CPSF6 by SYVN1, we obtained the mutants of CPSF6 (single sites of K79R, K161R, and K185R; double sites of K79R/K161R, K79R/K185R, and K161R/K185R; and triple sites of K79R/K161R/K185R) (Figure 5A). We first co-transfected Myc-CPSF6 (wild type [WT] or mutants), FLAG-SYVN1, and HA-K48 plasmids into HEK293T cells for 48 h and then infected them with VSV for 8 h. We first checked the degradation of CPSF6 protein and found that all of the CPSF6 mutants with K161R and K185R could not be degraded efficiently,

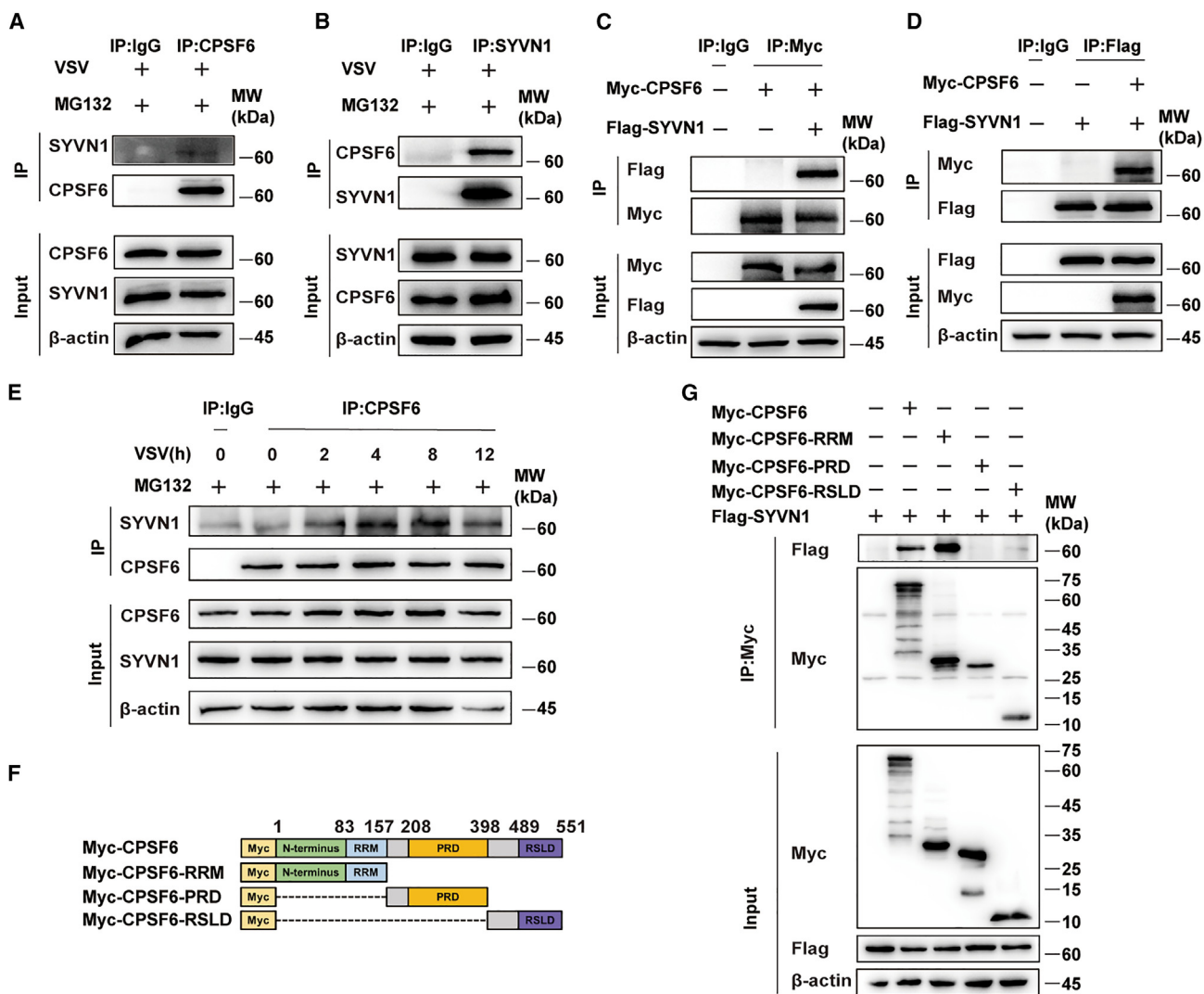


Figure 3. The interaction of SYVN1 with CPSF6

(A and B) Endogenous CPSF6 and SYVN1 can pull down each other. THP-1 cells were treated with MG132 (10 μM) and VSV infection for 8 h, and coIP was performed with anti-CPSF6 and anti-SYVN1.

(C and D) Overexpressed Myc-CPSF6 and FLAG-SYVN1 can pull down each other. Myc-CPSF6 and FLAG-SYVN1 were co-transfected into HEK293T cells for 48 h, and coIP was performed with anti-Myc and anti-FLAG, respectively.

(E) More SYVN1 can be pulled down by CPSF6 along with the infection time of VSV-EGFP. THP-1 cells were treated with MG132 (10 μM) and infected with VSV-EGFP. At different time points of infection, samples were collected, and coIP was performed with anti-CPSF6.

(F) Schematic of fragments of human CPSF6 fused with the Myc tag: WT, RNA recognition motif (RRM) domain, proline-rich domain (PRD), and arginine-serine-like domain (RSLD).

(G) Myc-CPSF6-RRM can pull down FLAG-SYVN1. HEK293T cells were co-transfected with FLAG-SYVN1 and Myc-CPSF6 fragments for 48 h, and coIP with anti-Myc was performed. Homologous IgG was used as a negative control.

suggesting that these two sites may be the target for ubiquitination of CPSF6 (Figure 5B). Furthermore, the ubiquitination modification of CPSF6 with K161R and K185R was significantly reduced compared to the WT (Figure 5C). To further confirm that SYVN1 mediates ubiquitination of CPSF6 at K161 and K185 through the ubiquitin chain linked to K48, we transfected Myc-CPSF6 (WT and mutant) plasmids into HEK293T cells with or without transfection of FLAG-SYVN1 plasmids. Consistently, the K48 ubiquitination modification on CPSF6 with K161R and

K185R mutations was significantly reduced compared to the WT (Figures 5D–5G).

Ubiquitination-mediated degradation of CPSF6 promotes APA and antivirus innate immunity of macrophages

With a THP-1 cell line with stable expression of shRNA specific to CPSF6, we validated that CPSF6 knockdown can significantly inhibit VSV replication (Figures S3A and S3B).

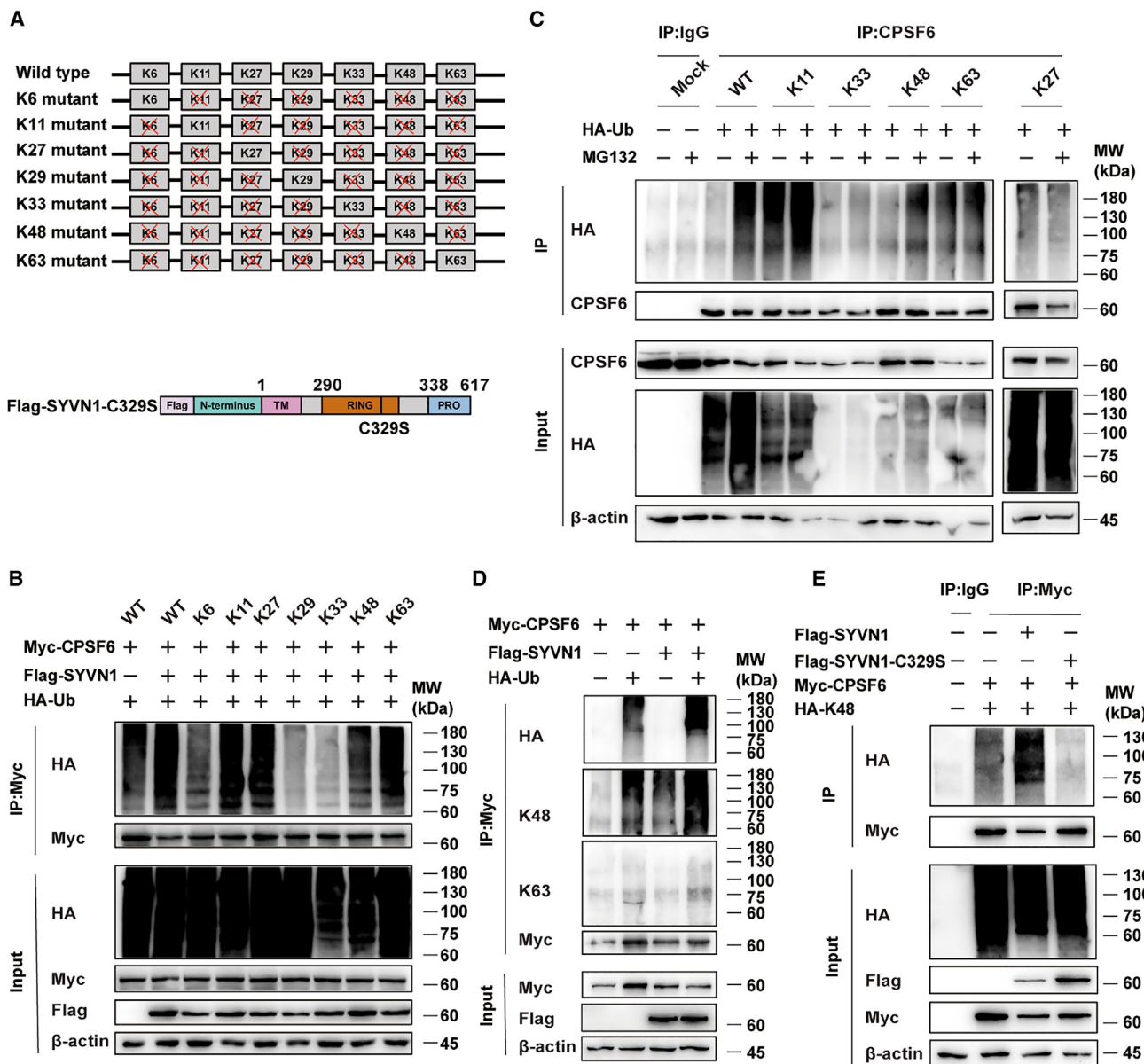


Figure 4. SYVN1 catalyzes K48-linked ubiquitination of CPSF6

- (A) Schematics of the HA-Ub mutant with single lysine only and the FLAG-SYVN1-C329S mutant.
- (B) Ubiquitination effects of Ub mutants on Myc-CPSF6 in HEK293T cells. The cells were co-transfected with Myc-CPSF6, FLAG-SYVN1, and HA-Ub (WT) or HA-Ub mutants for 48 h and infected with VSV, and IP was performed with anti-Myc following western blotting with anti-HA.
- (C) Ubiquitination effects of Ub mutants on endogenous CPSF6 in HEK293T cells. The cells were transfected with HA-Ub (WT) or HA-Ub mutants for 48 h, treated with MG132 (10 μM) or DMSO for 8 h, and infected with VSV, followed by IP with anti-CPSF6 and western blotting with anti-HA.
- (D) K48-linked ubiquitination of Myc-CPSF6 by FLAG-SYVN1 in HEK293T cells. The cells were co-transfected with Myc-CPSF6, FLAG-SYVN1, and HA-Ub (WT) and infected with VSV, followed by IP with anti-Myc and western blotting with anti-HA, anti-K48, and anti-K63.
- (E) The reduced effect of the SYVN1 C329S mutant on ubiquitination of Myc-CPSF6 in HEK293T cells. FLAG-SYVN1 and FLAG-SYVN1-C329S were co-transfected with Myc-CPSF6 and HA-K48, respectively, in HEK293T cells, followed by VSV infection and IP with anti-Myc and western blotting with anti-HA. Homologous IgG was used as a negative control.

To investigate the roles of CPSF6 degradation mediated by ubiquitination, we stably transfected the THP-1 cell line with WT and mutated (K161R, K185R, K161R/K185R) and infected them with VSV. After 12 h of VSV infection, 3' end sequencing by IVT-SAPAS was performed to compare the APA switching.

We found that the cells with stably expressed mutated CPSF6 (K161R, K185R, and K161R/K185R) showed more genes with longer 3' UTRs than the cells with stably expressed WT CPSF6 (Table S2). We also stably transfected the L929 cell line with the WT and mutated CPSF6 and infected them with VSV-EGFP.

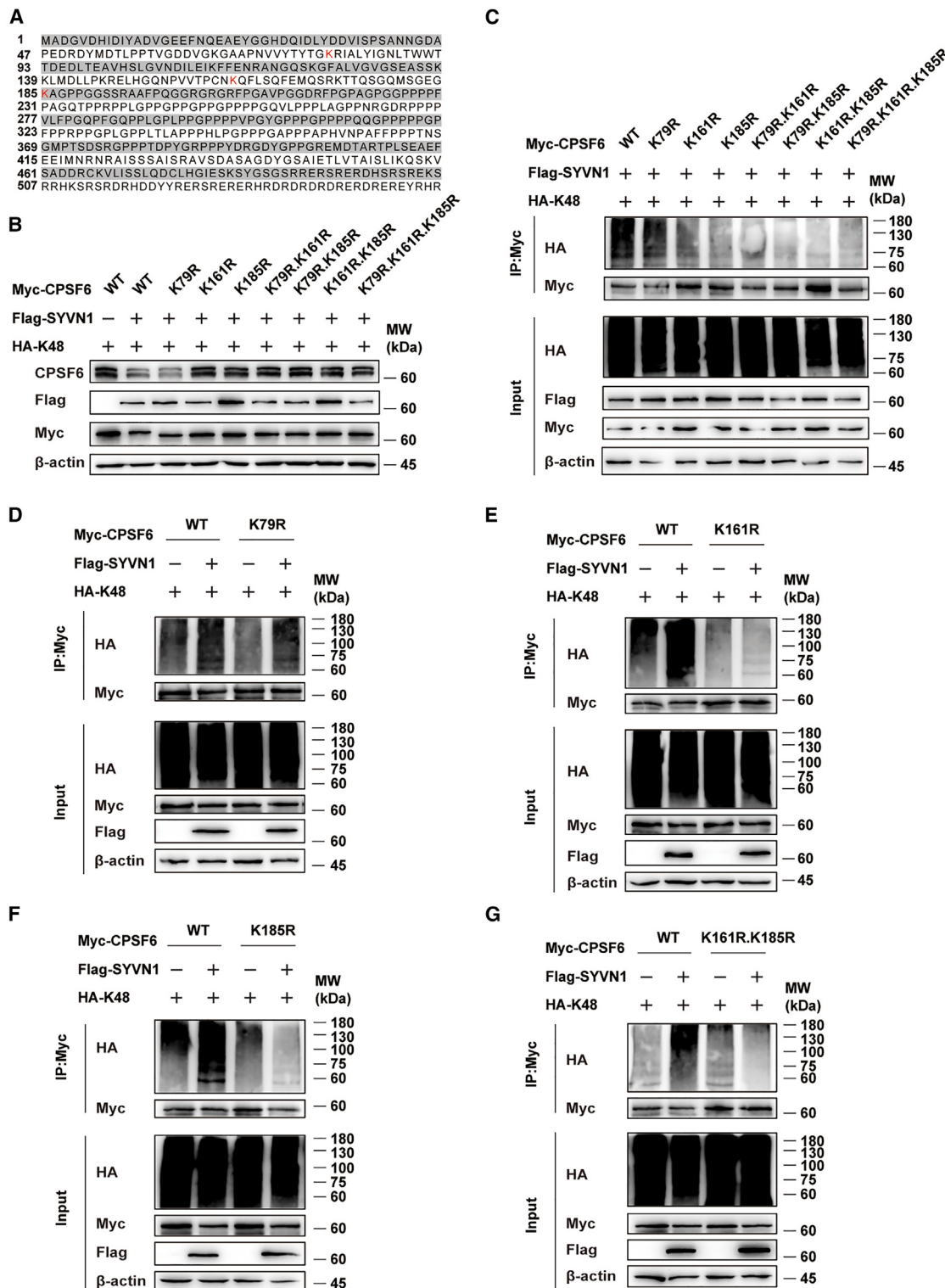


Figure 5. SYVN1 mediates K48-linked ubiquitination of CPSF6 at the sites of K161 and K185

(A) The potential ubiquitination sites (K79, K161, and K185) of CPSF6 predicted by UbiBrowser 2.0

(B) The effects of mutated potential ubiquitination sites (K103, K105, and K106) on CPSF6 degradation mediated by SYVN1. The single-, double-, and triple-sites mutants of Myc-CPSF6 were co-transfected with FLAG-SYVN1 and HA-K48-Ub in HEK293T cells, followed by VSV infection and western blot analysis with the indicated antibodies.

(legend continued on next page)

Both RT-qPCR and western blot analysis of VSV-G and VSV-M genes (Figure 6A), as well as fluorescence microscopy imaging of EGFP (Figure S3C), showed a considerable elevation in VSV loading in cells with a CPSF6 mutation (K185R and K161R/K185R) compared to the cells with WT CPSF6. We further measured the mRNA abundance of immune-related genes such as IL-6, RIG-I, Ifit3, and Isg15 (Figure 6B), and these genes showed significantly lower expression in the cells with stable expression of mutants of K185R and K161R/K185R than the cells with WT CPSF6.

In order to further demonstrate the role of the ubiquitin-dependent degradation of CPSF6 by SYVN1 in antiviral immunity, we obtained an L929 cell line with stable knockdown of SYVN1 and infected it with VSV-EGFP virions. Knockdown of SYVN1 can significantly improve the expression level of VSV-G protein (Figure 6C) and the fluorescence intensity of EGFP (Figure S3D), suggesting the promotion of viral replication. Moreover, knockdown of SYVN1 can also repress the expression of immune-related genes of Ifit3, RIG-I, and Isg15 (Figure 6D). We also treated THP-1 cells, PMs, and BMDMs with the SYVN1 inhibitor of LS-102. The inhibitor treatment resulted in a significant increase of VSV replication in all three kinds of cells (Figure 6E).

All of these results reveal that the ubiquitin-dependent degradation of CPSF6 mediated by SYVN1 can promote APA and anti-viral effects.

The MAVS pathway triggers SYVN1 nuclear import

SYVN1 is an E3 ubiquitin ligase that is predominantly located in the endoplasmic reticulum and plays an important role in the regulation of innate and adaptive immune responses.^{33–35} We found that the expression of SYVN1 protein and mRNA levels are not significantly changed after VSV infection in THP-1 cells ($p > 0.05$) (Figure S4A). Furthermore, CPSF6 is located in the nucleus to take part in 3' end processing. Then, we carried out immunofluorescence experiments to check the subcellular localization of SYVN1 in THP-1 cells upon VSV infection and found that SYVN1 is imported into the nucleus after 4 h of VSV infection in THP-1 cells. ImageJ analysis showed significantly more SYVN1 in the nucleus at 4 and 8 h of VSV infection than in the cells without VSV infection ($p < 0.001$) (Figure 7A). We also separated the nuclear and cytoplasmic fractions of THP-1 cells, and subsequent western blotting showed that SYVN1 in the nucleus was significantly increased after 8 h of viral infection (Figure 7B). This translocation of SYVN1 into the nucleus upon VSV infection was also validated in PMs (Figure 7C) and BMDMs (Figure 7D).

Nuclear pore complexes (NPCs), consisting of more than 30 nucleoporins (NUPs), are responsible for protein trafficking across the nuclear membrane.^{36,37} NUP153 has been found by mass spectrometry to be one of the potential substrates of SYVN1.³⁸ We overexpressed FLAG-SYVN1 and Myc-NUP153 in HEK293T cells, and subsequent coIP with anti-

FLAG shows that FLAG-SYVN1 can pull down Myc-NUP153 (Figure 7E), suggesting the interaction of these two proteins. We then disturbed the expression of NUP153 by overexpression and knockdown. The results show that overexpression of NUP153 in THP-1 cells can promote the degradation of CPSF6 after viral infection (Figure 7F), whereas knockdown of NUP153 can significantly inhibit the degradation of CPSF6 after VSV infection (Figure 7G).

To further understand the mechanism of SYVN1 translocation, we measured the post-translational modification of SYVN1 (Figures S4B and S4C). Phos-tag gel analysis did not show a significant mobility difference of SYVN1 upon VSV infection. However, IP of SYVN1 and subsequent western blotting showed that its methylation (asymmetric-dimethylarginine [ADMA] and monomethylarginine [MMA]) levels of SYVN1 are significantly reduced after VSV infection, suggesting that the reduction of methylation may be related to nuclear import of SYVN1.

To investigate the signaling pathway that activates the nuclear import of SYVN1 and the following degradation of CPSF6, we knocked down key recognition molecules and adapter proteins in the RLR and Toll-like receptor (TLR) pathways in THP-1 cells using siRNA (Figure S4D) and found that knockdown of MAVS and ZNFX1 can significantly inhibit CPSF6 protein degradation after virus infection (Figure 7H) without affecting the mRNA expression level of CPSF6 (Figure S4E). We then stably interfered with MAVS in A549 cells using shRNA (Figure S4F). Immunofluorescence analysis showed that MAVS knockdown can inhibit SYVN1 entry into the nucleus, and ANOVA also revealed that there is a significant interaction effect of MAVS and VSV infection on nuclear import of SYVN1 ($p < 0.0001$) (Figure 7I).

CoIP with an antibody against SYVN1 in THP-1 cells with VSV infection showed that MAVS can be pulled down by SYVN1 and that the interaction was elevated with increasing duration time of virus infection (Figure S4G). We also investigated the effect of MAVS on ubiquitination degradation of CPSF6 in A549 cells with stable knockdown of MAVS, and the result revealed that the knockdown of MAVS can reduce the ubiquitination modification level of endogenous CPSF6 (Figure S4H), which is in accordance with the results of knockdown of SYVN1.

Furthermore, we analyzed the effect of MAVS on CPSF6 degradation in L929 cells with the stably transfected WT and mutants of CPSF6 after VSV infection. It is obvious that the CPSF6 protein level is lower in cells with the WT than in cells with mutants of K185R and K161R/K185R with VSV infection (Figure S4I), whereas knockdown of MAVS can eliminate the difference. This suggests that MAVS activates the degradation of CPSF6 upon VSV infection.

All of this evidence illustrates a new mechanism whereby MAVS activated by VSV infection promotes the nuclear import of SYVN1 mediated by NUP153, and then SYVN1 ubiquitinates and degrades CPSF6, which then promotes an antivirus effect by regulating APA switching.

(C) HEK293T cells were co-transfected with FLAG-SYVN1, HA-K48, and WT or mutant Myc-CPSF6 and infected with VSV after treatment with MG132 for 8 h, followed by IP with anti-Myc and western blotting with anti-HA.

(D–G) The effect of FLAG-SYVN1 on K48-linked ubiquitination of CPSF6 mutants. HEK293T cells were co-transfected with the WT or mutants of Myc-CPSF6, HA-K48, and FLAG-SYVN1 or FLAG, treated with MG132, and infected with VSV, followed by IP with anti-Myc and western blotting with anti-HA.

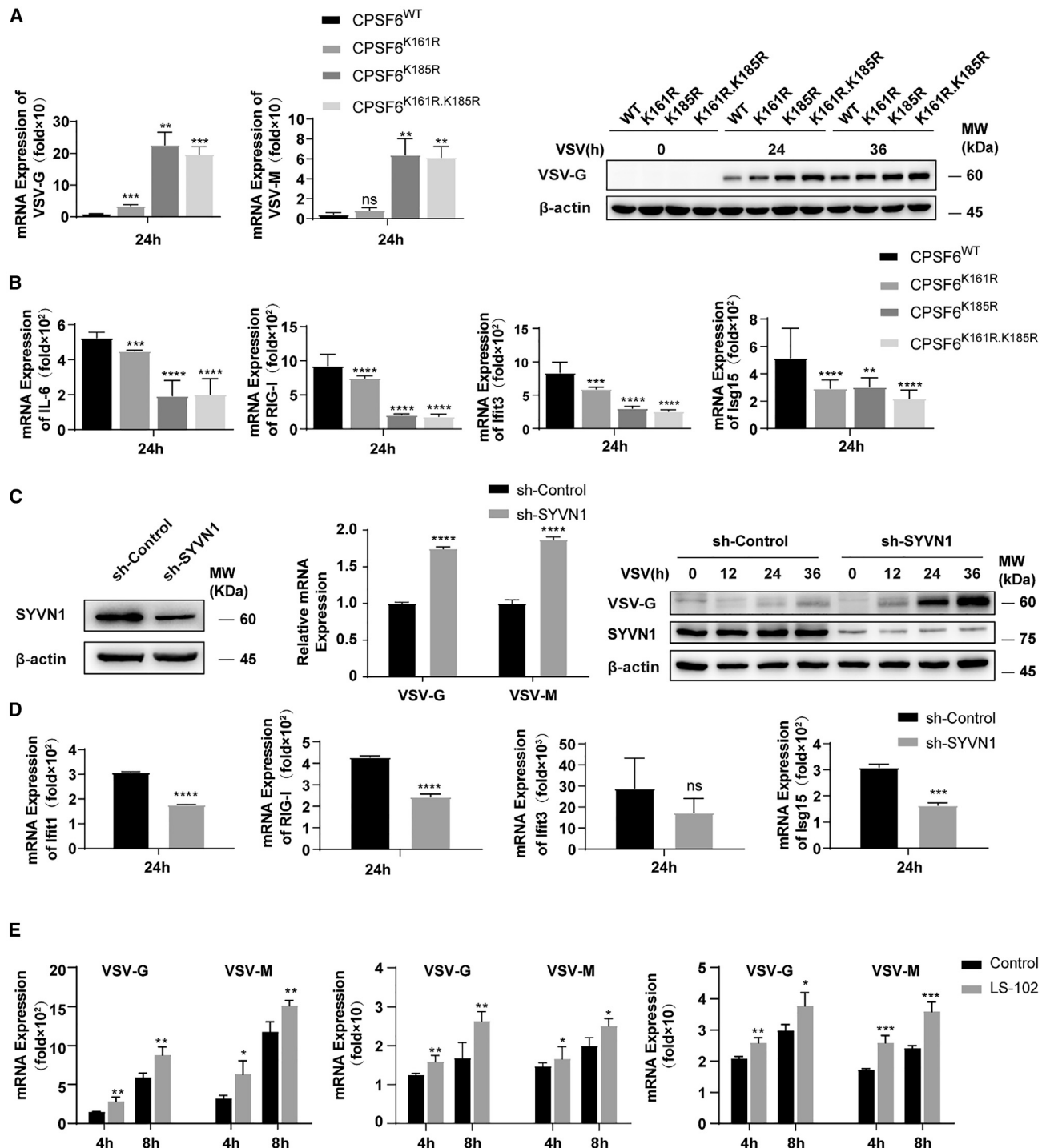


Figure 6. Anti-virus effect of SYVN1 through ubiquitination of CPSF6

(A) The effect of CPSF6 ubiquitination site mutation on VSV replication. Left: RT-qPCR analysis of VSV-G in L929 cells with stably expressed WT and mutants of CPSF6 at 24 h of VSV-EGFP infection. Error bars indicate SD ($n = 3$ replicates). Right: western blot analysis of VSV-G protein at 24 and 36 h of infection. ns, not significant; ** $p < 0.01$, *** $p < 0.001$, **** $p < 0.0001$ with t test and Bonferroni correction.

(B) RT-qPCR analysis of the immune-related genes in L929 cells with stable expression of the WT and mutants of CPSF6 at 24 h of VSV-EGFP infection. Error bars indicate SD ($n = 3$ replicates). ** $p < 0.01$, *** $p < 0.001$ with t test and Bonferroni correction.

(legend continued on next page)

DISCUSSION

It is widely known that immune cells switch to transcriptome-wide shortened 3' UTRs due to APA in response to foreign antigens and that the APA switching can promote both adaptive and innate immunity. The expression level changes of 3' end processing factors such as CstF64 and CPSF6 play important roles in the APA switching. However, the molecular mechanisms of the expression changes of these factors remain to be determined. Here, we found that the protein but not mRNA level of CPSF6 is remarkably reduced in response to VSV infection in macrophages. MAVS activated by virus infection promotes transportation of the E3 ligase SYVN1 into the nucleus from the cytoplasm, and then SYVN1 catalyzes the K48-linked ubiquitination of CPSF6, resulting in the degradation of CPSF6 by the proteasome. The reduced level of CPSF6 leads to APA switching and promotes antivirus immunity.

SYVN1, an endoplasmic reticulum (ER)-resident RING E3 ligase, has been found to be involved in immune regulation and inflammation by targeting several proteins at the ER region. It is upregulated in synovial fibroblasts from patients with rheumatoid arthritis, which can induce synovial cell outgrowth.³⁹ SYVN1 can promote the clonal expansion of activated CD4⁺ T cells by targeting p27, and its elevated expression is associated with multiple sclerosis.³⁴ SYVN1 enhances TLR-induced inflammatory cytokine production in macrophages during bacterial infection by targeting Usp15 through K27-linked ubiquitination and subsequent activation of nuclear factor κ B.⁴⁰ SYVN1 can also promote inflammasome-induced pyroptosis through K27-linked ubiquitination of GSDMD.³² Here, we found that SYVN1 could modify CPSF6 with K48-linked ubiquitination in macrophages upon VSV infection, and the reduced protein level of CPSF6 led to transcriptome-wide APA switching and enhanced the antivirus effect. CPSF6 is located in the nucleus to function as a 3' end-processing factor, so how SYVN1 can interact and ubiquitinate became the question that should be resolved. P53 has also been found to be a substance of SYVN1, and overexpression of p53 and SYVN1 revealed that p53 predominantly colocalizes with SYVN1 in the ER at perinuclear regions.⁴¹ With an immunofluorescence assay and separation of nuclear and cytoplasmic fractions, we observed significant nuclear import of SYVN1 in the THP-1 cell line and mouse primary PMs and BMDMs upon VSV infection (Figures 7A–7D). We further identified the interaction of SYVN1 and NUP153 (a component of the NPC) and found that NUP153 can promote CPSF6 degradation upon VSV infection through experiments of overexpression and knockdown of NUP153 (Figures 7F and 7G). All of these observations reveal that the translocation of SYVN1 upon VSV infection enables it to target CPSF6 in the nucleus, which is the first evidence showing that SYVN1 can function to ubiquitinate the protein located in the nucleus.

CPSF6 plays an important role in APA regulation by promoting the distal poly(A) sites.¹⁷ Our group has found the transcriptome wide shorter 3' UTR in macrophages of human and mouse upon VSV infection,⁹ and this is caused by the reduced expression level of CPSF6.¹¹ Here, we further demonstrated that CPSF6 is polyubiquitinated at the K161 and K185 residues by SYVN1 in macrophages upon VSV infection, resulting in the degradation and reduction of its protein level without changes of the mRNA expression level. Post-translational changes of 3' end-processing factors have attracted much attention in recent years. CPSF6 has been found to be extensively phosphorylated in cells, and the modification could impact its subcellular location and interaction with FIP1L1, leading to APA switching.^{17,42,43} We further identified that the phosphorylation of CPSF6 can attenuate its phase separation and then promote the proximal poly(A) sites in cancer cells.⁴⁴ Moreover, phase separation changes of PABPN1 have been observed in cancer cells and growing mouse oocytes.⁴⁵ Ubiquitination of the 3' end-processing factor PCF11 has been found to lead to APA site switching and tumorigenesis.⁴⁶ All of this suggests that post-translational regulation of 3' end-processing factors is an important way of APA regulation and deserves to be investigated in depth.

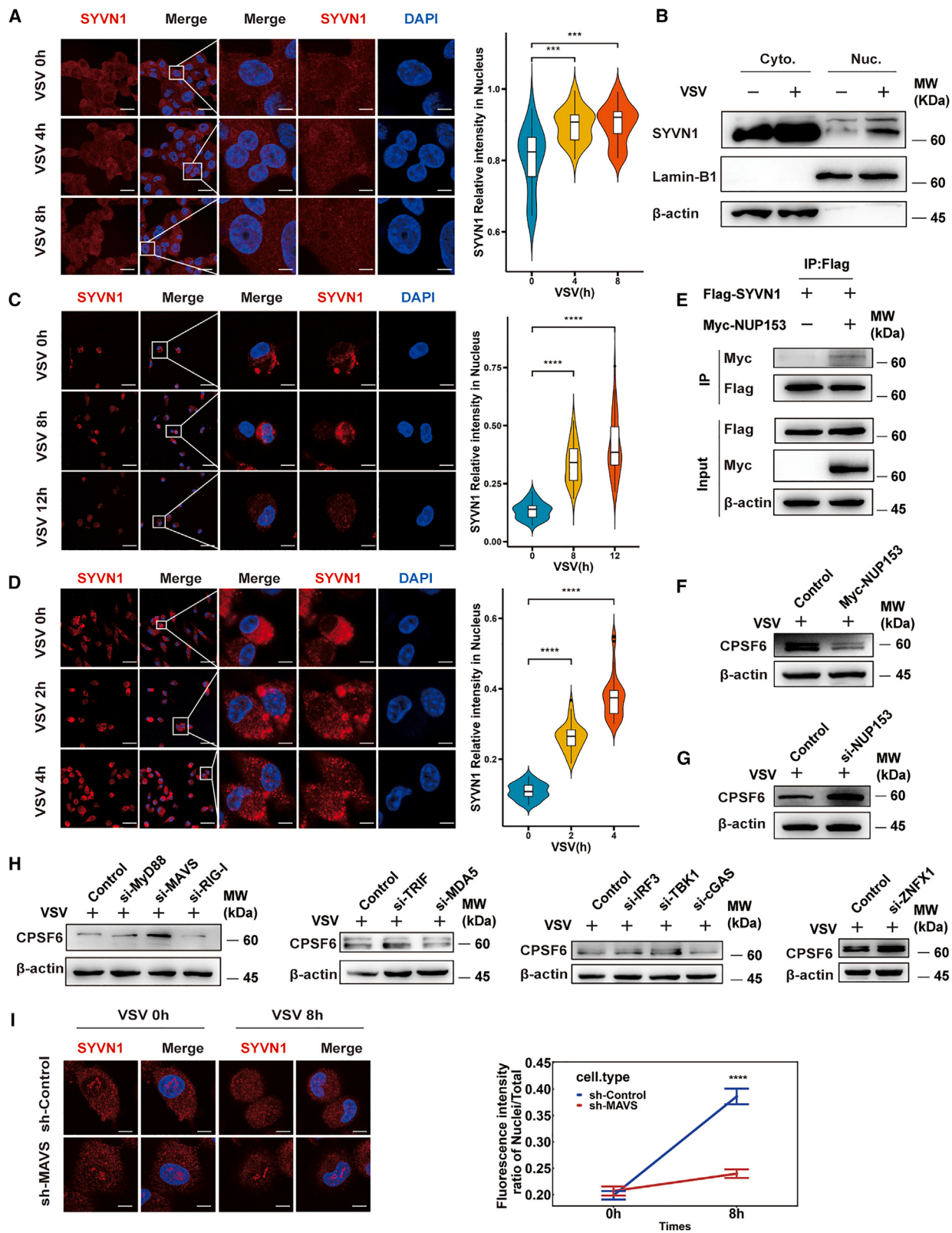
The RLR/MAVS pathway plays an essential role in immune responses to RNA viruses.³ Here, our results reveal that the MAVS activated in macrophages by VSV infection promotes the nuclear import of SYVN1, which then ubiquitinates CPSF6. This provides a new mechanism of innate immune responses to RNA viruses. We investigated the effect of RLRs of RIG-I, MDA5, and ZNFX1 on CPSF6 degradation. Among the three receptors, only knockdown of ZNFX1 could significantly rescue degradation of the CPSF6 protein level upon VSV infection (Figure 7H). Treatment of THP-1 cells with 5ppp-hpRNA (a specific agonist of RIG-I) did not promote the degradation of CPSF6 either (Figure S4J). Our group has identified that ZNFX1 can sense viral RNA, interact with MAVS, and then induce the antivirus responses independent of RIG-I and MDA5.⁴⁷ This suggests that ZNFX1 recognizes virus RNA and activates MAVS, and then the activated MAVS initiates the nuclear import of SYVN1.

Actually, we also found a protein but not mRNA level reduction of CPSF6 in THP-1 cells with treatment of poly(dA:dT) (Figure 1F) and HSV-1 DNA virus infection (Figure S1D), suggesting that DNA viruses can also lead to a reduction of CPSF6 protein levels. The molecular mechanism of the CPSF6 protein level reduction upon HSV-1 infection should be different from that by VSV infection. HSV-1 infection could disrupt transcription termination by interaction of the virus ICP27 with the CPSF complex.^{48,49} Even more interesting is that HSV-1 also led to a preference of the proximal poly(A) sites in both ICP27-dependent and

(C) Knockdown of SYVN1 by shRNA represses VSV-EGFP replication. Left: knockdown of SYVN1 by stably expressed shRNA in L929 cells. Center: RT-qPCR analysis of mRNA expression levels of VSV-G and -M genes at 8 h of VSV-EGFP infection ($n = 3$ replicates). Right: immunoblot detection of VSV-G protein expression at different time points of VSV infection. Error bars indicate SD. *** $p < 0.0001$ with t test.

(D) RT-qPCR detection of immune-related genes after 24 h of VSV infection in L929 cells with stable knockdown of SYVN1. Error bars indicate SD ($n = 3$ replicates). ** $p < 0.001$, *** $p < 0.0001$ with t test.

(E) The expression levels of VSV-G and -M after treatment with LS-102 for 4 h and VSV infection for 4 and 8 h. Left: THP-1 cells. Center: PMs. Right: BMDMs. Error bars indicate SD ($n = 3$ replicates). * $p < 0.05$, ** $p < 0.01$, *** $p < 0.001$ with t test.



(legend on next page)

-independent ways and that ΔICP27 HSV-1 infection resulted in more APA switching events than the WT virus.⁵⁰ Then, the CPSF6 protein reduction in response to HSV-1 infection may be related to APA switching upon ΔICP27 HSV-1 infection, and the coordinated effect of CPSF6 reduction and ICP27 on APA regulation should be investigated further.

In conclusion, the MAVS pathway activates the nuclear import of SYVN1, which ubiquitinates CPSF6, leading to a reduced level of CPSF6 protein, subsequently promoting APA switching and antivirus effects. Our findings provide insights into APA regulation at the level of post-translational modification and innate immune response to RNA virus infection.

Limitations of the study

Some questions remain to be answered. Our study found an effect of the MAVS/SYVN1 pathway on CPSF6 degradation upon VSV infection. However, the mechanism of activation of MAVS by ZNFX1 in this pathway still remains unclear. Although we identified the demethylation of SYVN1 upon VSV infection, its regulation mechanism and effect on promoting nuclear import should also be investigated further.

RESOURCE AVAILABILITY

Lead contact

Requests for further information and resources should be directed to and will be fulfilled by the lead contact, Anlong Xu (lssxal@mail.sysu.edu.cn).

Materials availability

This study did not generate new unique reagents.

Data and code availability

- All APA sequencing data have been deposited at the NCBI GEO and China National Center for Bioinformation and are publicly available as of the date of publication. Accession numbers are listed in the [key resources table](#).
- This paper does not report original code.
- Any additional information required to reanalyze the data reported in this paper is available from the [lead contact](#) upon request.

ACKNOWLEDGMENTS

This work was supported by the National Key Research and Development Program of China (2022YFA1103900), the National Natural Science Foundation of China (32470586), the Guangdong Science and Technology Department (2023B1212060028), and the Joint Funds of National Natural Science Foundation of China (U23A6012).

Figure 7. MAVS activates nuclear import of SYVN1 through NUP153

- (A) SYVN1 is translocated into the nucleus in THP-1 cells upon VSV-EGFP infection. Left: confocal image of endogenous SYVN1 with anti-SYVN1. Right: violin plot of the relative fluorescence intensity of SYVN1 in the nucleus of different cells using ImageJ. Scale bars: 5 and 20 μm. t test: ***p < 0.0001 (n = 21 cells).
- (B) Western blot analysis of SYVN1 in fractions of the nucleus and cytoplasm of THP-1 cells infected with VSV for 8 h.
- (C) Nucleus translocation of SYVN1 in PMs with infection of VSV-EGFP. Right: violin plot of the relative fluorescence intensity of SYVN1. Scale bars: 5 and 20 μm. t test: ***p < 0.0001 (n = 37 cells).
- (D) Nucleus translocation of SYVN1 in BMDMs with infection of VSV-EGFP. Right: violin plot of the relative fluorescence intensity of SYVN1. Scale bars: 5 and 20 μm t test: ***p < 0.0001 (n = 43 cells).
- (E) CoIP analysis of Myc-NUP153 and FLAG-SYVN1 in HEK293 cells upon VSV-EGFP infection.
- (F and G) Western blot analysis of CPSF6 protein expression in THP-1 cells with NUP153 overexpression and knockdown after VSV-EGFP infection.
- (H) Western blot analysis of CPSF6 in THP-1 cells with knockdown of PRRs pathway genes upon VSV-EGFP infection.
- (I) MAVS triggers nuclear imports of SYVN1 upon VSV-EGFP infection. Left: confocal image of endogenous SYVN1 in A549 cells with knockdown of MAVS upon VSV-EGFP infection. Right: ANOVA of the interaction effect of virus infection and MAVS on the relative fluorescence intensity of SYVN1 in the nucleus. Scale bar, 20 μm. two-way ANOVA was performed (n = 27 cells). ***p < 0.0001.

AUTHOR CONTRIBUTIONS

A.X. and Y.F. conceived the study. X.L. and Y.F. designed the experiments. X.L., C.Liu, R.W., and Z.H. performed the experiments. X.L., C.Liu, K.D., X.O., C.Liang, and Y.Fu. performed the data analysis. X.L., Y.F., and A.X. wrote the manuscript. All authors approved the submission.

DECLARATION OF INTERESTS

The authors declare no competing interests.

STAR METHODS

Detailed methods are provided in the online version of this paper and include the following:

- KEY RESOURCES TABLE
- EXPERIMENTAL MODEL AND STUDY PARTICIPANT DETAILS
 - Animals
 - Cell culture
- METHOD DETAILS
 - RNA extraction and qRT-PCR
 - Virus infection
 - Analogue stimulation
 - Proteasome and autophagy inhibitor treatment
 - Plasmid transfection
 - Stable knockdown or overexpression cell lines
 - Western blot
 - Phos-tag SDS PAGE and western blotting
 - Immunoprecipitation analysis
 - Immunofluorescence
 - Antibodies
 - IVT-SAPAS library
- QUANTIFICATION AND STATISTICAL ANALYSIS

SUPPLEMENTAL INFORMATION

Supplemental information can be found online at <https://doi.org/10.1016/j.celrep.2025.115276>.

Received: July 24, 2024

Revised: December 3, 2024

Accepted: January 16, 2025

Published: February 13, 2025

REFERENCES

- Wu, J., and Chen, Z.J. (2014). Innate immune sensing and signaling of cytosolic nucleic acids. *Annu. Rev. Immunol.* 32, 461–488. <https://doi.org/10.1146/annurev-immunol-032713-120156>.

2. Kawai, T., and Akira, S. (2011). Toll-like receptors and their crosstalk with other innate receptors in infection and immunity. *Immunity* 34, 637–650. <https://doi.org/10.1016/j.jimmuni.2011.05.006>.
3. Ablasser, A., and Hur, S. (2020). Regulation of cGAS- and RLR-mediated immunity to nucleic acids. *Nat. Immunol.* 21, 17–29. <https://doi.org/10.1038/s41590-019-0556-1>.
4. Mitschka, S., and Mayr, C. (2022). Context-specific regulation and function of mRNA alternative polyadenylation. *Nat. Rev. Mol. Cell Biol.* 23, 779–796. <https://doi.org/10.1038/s41580-022-00507-5>.
5. Tian, B., and Manley, J.L. (2017). Alternative polyadenylation of mRNA precursors. *Nat. Rev. Mol. Cell Biol.* 18, 18–30. <https://doi.org/10.1038/nrm.2016.116>.
6. Di Giammartino, D.C., Nishida, K., and Manley, J.L. (2011). Mechanisms and consequences of alternative polyadenylation. *Mol. Cell* 43, 853–866. <https://doi.org/10.1016/j.molcel.2011.08.017>.
7. Sandberg, R., Neilson, J.R., Sarma, A., Sharp, P.A., and Burge, C.B. (2008). Proliferating cells express mRNAs with shortened 3' untranslated regions and fewer microRNA target sites. *Science* 320, 1643–1647.
8. Qiu, F., Fu, Y., Lu, C., Feng, Y., Wang, Q., Huo, Z., Jia, X., Chen, C., Chen, S., and Xu, A. (2017). Small Nuclear Ribonucleoprotein Polypeptide A-Mediated Alternative Polyadenylation of STAT5B during Th1 Cell Differentiation. *J. Immunol.* 199, 3106–3115. <https://doi.org/10.4049/jimmunol.1601872>.
9. Jia, X., Yuan, S., Wang, Y., Fu, Y., Ge, Y., Ge, Y., Lan, X., Feng, Y., Qiu, F., Li, P., et al. (2017). The role of alternative polyadenylation in the antiviral innate immune response. *Nat. Commun.* 8, 14605. <https://doi.org/10.1038/ncomms14605>.
10. Huang, G., Huang, S., Wang, R., Yan, X., Li, Y., Feng, Y., Wang, S., Yang, X., Chen, L., Li, J., et al. (2016). Dynamic Regulation of Tandem 3' Untranslated Regions in Zebrafish Spleen Cells during Immune Response. *J. Immunol.* 196, 715–725. <https://doi.org/10.4049/jimmunol.1500847>.
11. Ge, Y., Huang, J., Chen, R., Fu, Y., Ling, T., Ou, X., Rong, X., Cheng, Y., Lin, Y., Zhou, F., et al. (2024). Downregulation of CPSF6 leads to global mRNA 3' UTR shortening and enhanced antiviral immune responses. *PLoS Pathog.* 20, e1012061. <https://doi.org/10.1371/journal.ppat.1012061>.
12. Boreikaité, V., and Passmore, L.A. (2023). 3'-End Processing of Eukaryotic mRNA: Machinery, Regulation, and Impact on Gene Expression. *Annu. Rev. Biochem.* 92, 199–225. <https://doi.org/10.1146/annurev-biochem-052521-012445>.
13. Takagaki, Y., Seipelt, R.L., Peterson, M.L., and Manley, J.L. (1996). The polyadenylation factor CstF-64 regulates alternative processing of IgM heavy chain pre-mRNA during B cell differentiation. *Cell* 87, 941–952. [https://doi.org/10.1016/s0092-8674\(00\)82000-0](https://doi.org/10.1016/s0092-8674(00)82000-0).
14. Takagaki, Y., and Manley, J.L. (1998). Levels of polyadenylation factor CstF-64 control IgM heavy chain mRNA accumulation and other events associated with B cell differentiation. *Mol. Cell* 2, 761–771. [https://doi.org/10.1016/s1097-2765\(00\)80291-9](https://doi.org/10.1016/s1097-2765(00)80291-9).
15. Chuvpilo, S., Zimmer, M., Kerstan, A., Glöckner, J., Avots, A., Escher, C., Fischer, C., Inashkina, I., Jankevics, E., Berberich-Siebelt, F., et al. (1999). Alternative polyadenylation events contribute to the induction of NF-ATc in effector T cells. *Immunity* 10, 261–269.
16. Brown, K.M., and Gilmartin, G.M. (2003). A mechanism for the regulation of pre-mRNA 3' processing by human cleavage factor Im. *Mol. Cell* 12, 1467–1476. [https://doi.org/10.1016/s1097-2765\(03\)00453-2](https://doi.org/10.1016/s1097-2765(03)00453-2).
17. Zhu, Y., Wang, X., Forouzmand, E., Jeong, J., Qiao, F., Sowd, G.A., Engelmann, A.N., Xie, X., Hertel, K.J., and Shi, Y. (2018). Molecular Mechanisms for CFIm-Mediated Regulation of mRNA Alternative Polyadenylation. *Mol. Cell* 69, 62–74.e4. <https://doi.org/10.1016/j.molcel.2017.11.031>.
18. Ghosh, S., Ataman, M., Bak, M., Börsch, A., Schmidt, A., Buczak, K., Martin, G., Dimitriades, B., Herrmann, C.J., Kanitz, A., and Zavolan, M. (2022). CFIm-mediated alternative polyadenylation remodels cellular signaling and miRNA biogenesis. *Nucleic Acids Res.* 50, 3096–3114. <https://doi.org/10.1093/nar/gkac114>.
19. Li, W., You, B., Hoque, M., Zheng, D., Luo, W., Ji, Z., Park, J.Y., Gunderson, S.I., Kalsotra, A., Manley, J.L., and Tian, B. (2015). Systematic profiling of poly(A)+ transcripts modulated by core 3' end processing and splicing factors reveals regulatory rules of alternative cleavage and polyadenylation. *PLoS Genet.* 11, e1005166. <https://doi.org/10.1371/journal.pgen.1005166>.
20. Masamha, C.P., Xia, Z., Yang, J., Albrecht, T.R., Li, M., Shyu, A.B., Li, W., and Wagner, E.J. (2014). CFIm25 links alternative polyadenylation to glioblastoma tumour suppression. *Nature* 510, 412–416. <https://doi.org/10.1038/nature13261>.
21. Tan, S., Zhang, M., Shi, X., Ding, K., Zhao, Q., Guo, Q., Wang, H., Wu, Z., Kang, Y., Zhu, T., et al. (2021). CPSF6 links alternative polyadenylation to metabolism adaption in hepatocellular carcinoma progression. *J. Exp. Clin. Cancer Res.* 40, 85. <https://doi.org/10.1186/s13046-021-01884-z>.
22. Fu, Y., Ge, Y., Sun, Y., Liang, J., Wan, L., Wu, X., and Xu, A. (2015). IVT-SAPAS: Low-Input and Rapid Method for Sequencing Alternative Polyadenylation Sites. *PLoS One* 10, e0145477. <https://doi.org/10.1371/journal.pone.0145477>.
23. Fu, Y., Sun, Y., Li, Y., Li, J., Rao, X., Chen, C., and Xu, A. (2011). Differential genome-wide profiling of tandem 3' UTRs among human breast cancer and normal cells by high-throughput sequencing. *Genome Res.* 21, 741–747. <https://doi.org/10.1101/gr.115295.110>.
24. Schwahnässer, B., Busse, D., Li, N., Dittmar, G., Schuchhardt, J., Wolf, J., Chen, W., and Selbach, M. (2011). Global quantification of mammalian gene expression control. *Nature* 473, 337–342. <https://doi.org/10.1038/nature10098>.
25. Zhao, L., Zhao, J., Zhong, K., Tong, A., and Jia, D. (2022). Targeted protein degradation: mechanisms, strategies and application. *Signal Transduct. Targeted Ther.* 7, 113. <https://doi.org/10.1038/s41392-022-00966-4>.
26. Lee, D.H., and Goldberg, A.L. (1998). Proteasome inhibitors: valuable new tools for cell biologists. *Trends Cell Biol.* 8, 397–403. [https://doi.org/10.1016/s0962-8924\(98\)01346-4](https://doi.org/10.1016/s0962-8924(98)01346-4).
27. Devis-Jauregui, L., Eritja, N., Davis, M.L., Matias-Guiu, X., and Llobet-Navàs, D. (2021). Autophagy in the physiological endometrium and cancer. *Autophagy* 17, 1077–1095. <https://doi.org/10.1080/15548627.2020.1752548>.
28. Glickman, M.H., and Ciechanover, A. (2002). The ubiquitin-proteasome proteolytic pathway: destruction for the sake of construction. *Physiol. Rev.* 82, 373–428. <https://doi.org/10.1152/physrev.00027.2001>.
29. Pohl, C., and Dikic, I. (2019). Cellular quality control by the ubiquitin-proteasome system and autophagy. *Science (New York, N.Y.)* 366, 818–822. <https://doi.org/10.1126/science.aax3769>.
30. Yagishita, N., Aratani, S., Leach, C., Amano, T., Yamano, Y., Nakatani, K., Nishioka, K., and Nakajima, T. (2012). RING-finger type E3 ubiquitin ligase inhibitors as novel candidates for the treatment of rheumatoid arthritis. *Int. J. Mol. Med.* 30, 1281–1286. <https://doi.org/10.3892/ijmm.2012.1129>.
31. Chau, V., Tobias, J.W., Bachmair, A., Marriott, D., Ecker, D.J., Gonda, D.K., and Varshavsky, A. (1989). A multiubiquitin chain is confined to specific lysine in a targeted short-lived protein. *Science (New York, N.Y.)* 243, 1576–1583. <https://doi.org/10.1126/science.2538923>.
32. Shi, Y., Yang, Y., Xu, W., Shi, D., Xu, W., Fu, X., Lv, Q., Xia, J., and Shi, F. (2022). E3 ubiquitin ligase SYVN1 is a key positive regulator for GSDMD-mediated pyroptosis. *Cell Death Dis.* 13, 106. <https://doi.org/10.1038/s41419-022-04553-x>.
33. Xu, Y., and Fang, D. (2020). Endoplasmic reticulum-associated degradation and beyond: The multitasking roles for HRD1 in immune regulation and autoimmunity. *J. Autoimmun.* 109, 102423. <https://doi.org/10.1016/j.jaut.2020.102423>.
34. Xu, Y., Zhao, F., Qiu, Q., Chen, K., Wei, J., Kong, Q., Gao, B., Melo-Cardenas, J., Zhang, B., Zhang, J., et al. (2016). The ER membrane-anchored

- ubiquitin ligase Hrd1 is a positive regulator of T-cell immunity. *Nat. Commun.* 7, 12073. <https://doi.org/10.1038/ncomms12073>.
35. Yang, H., Qiu, Q., Gao, B., Kong, S., Lin, Z., and Fang, D. (2014). Hrd1-mediated BLIMP-1 ubiquitination promotes dendritic cell MHCII expression for CD4 T cell priming during inflammation. *J. Exp. Med.* 211, 2467–2479. <https://doi.org/10.1084/jem.20140283>.
 36. Otsuka, S., Iwasaka, S., Yoneda, Y., Takeyasu, K., and Yoshimura, S.H. (2008). Individual binding pockets of importin-beta for FG-nucleoporins have different binding properties and different sensitivities to RanGTP. *Proc. Natl. Acad. Sci. USA* 105, 16101–16106. <https://doi.org/10.1073/pnas.0802647105>.
 37. Ben-Efraim, I., and Gerace, L. (2001). Gradient of increasing affinity of importin beta for nucleoporins along the pathway of nuclear import. *J. Cell Biol.* 152, 411–417. <https://doi.org/10.1083/jcb.152.2.411>.
 38. Ye, Y., Baek, S.H., Ye, Y., and Zhang, T. (2018). Proteomic characterization of endogenous substrates of mammalian ubiquitin ligase Hrd1. *Cell Biosci.* 8, 46. <https://doi.org/10.1186/s13578-018-0245-z>.
 39. Amano, T., Yamasaki, S., Yagishita, N., Tsuchimochi, K., Shin, H., Kawahara, K.i., Aratani, S., Fujita, H., Zhang, L., Ikeda, R., et al. (2003). Synoviolin/Hrd1, an E3 ubiquitin ligase, as a novel pathogenic factor for arthropathy. *Genes Dev.* 17, 2436–2449. <https://doi.org/10.1101/gad.1096603>.
 40. Lu, Y., Qiu, Y., Chen, P., Chang, H., Guo, L., Zhang, F., Ma, L., Zhang, C., Zheng, X., Xiao, J., et al. (2019). ER-localized Hrd1 ubiquitinates and inactivates Usp15 to promote TLR4-induced inflammation during bacterial infection. *Nat. Microbiol.* 4, 2331–2346. <https://doi.org/10.1038/s41564-019-0542-2>.
 41. Yamasaki, S., Yagishita, N., Sasaki, T., Nakazawa, M., Kato, Y., Yamadera, T., Bae, E., Toriyama, S., Ikeda, R., Zhang, L., et al. (2007). Cytoplasmic destruction of p53 by the endoplasmic reticulum-resident ubiquitin ligase 'Synoviolin'. *EMBO J.* 26, 113–122. <https://doi.org/10.1038/sj.emboj.7601490>.
 42. Tang, H.W., Hu, Y., Chen, C.L., Xia, B., Zirin, J., Yuan, M., Asara, J.M., Rabinow, L., and Perrimon, N. (2018). The TORC1-Regulated CPA Complex Rewires an RNA Processing Network to Drive Autophagy and Metabolic Reprogramming. *Cell Metabol.* 27, 1040–1054.e8. <https://doi.org/10.1016/j.cmet.2018.02.023>.
 43. Jang, S., Cook, N.J., Pye, V.E., Bedwell, G.J., Dudek, A.M., Singh, P.K., Cherepanov, P., and Engelman, A.N. (2019). Differential role for phosphorylation in alternative polyadenylation function versus nuclear import of SR-like protein CPSF6. *Nucleic Acids Res.* 47, 4663–4683. <https://doi.org/10.1093/nar/gkz206>.
 44. Liu, S., Wu, R., Chen, L., Deng, K., Ou, X., Lu, X., Li, M., Liu, C., Chen, S., Fu, Y., and Xu, A. (2023). CPSF6 regulates alternative polyadenylation and proliferation of cancer cells through phase separation. *Cell Rep.* 42, 113197. <https://doi.org/10.1016/j.celrep.2023.113197>.
 45. Dai, X.X., Pi, S.B., Zhao, L.W., Wu, Y.W., Shen, J.L., Zhang, S.Y., Sha, Q.Q., and Fan, H.Y. (2022). PABPN1 functions as a hub in the assembly of nuclear poly(A) domains that are essential for mouse oocyte development. *Sci. Adv.* 8, eabn9016. <https://doi.org/10.1126/sciadv.abn9016>.
 46. Yang, S.W., Li, L., Connelly, J.P., Porter, S.N., Kodali, K., Gan, H., Park, J.M., Tacer, K.F., Tillman, H., Peng, J., et al. (2020). A Cancer-Specific Ubiquitin Ligase Drives mRNA Alternative Polyadenylation by Ubiquitinating the mRNA 3' End Processing Complex. *Mol. Cell* 77, 1206–1221.e7. <https://doi.org/10.1016/j.molcel.2019.12.022>.
 47. Wang, Y., Yuan, S., Jia, X., Ge, Y., Ling, T., Nie, M., Lan, X., Chen, S., and Xu, A. (2019). Mitochondria-localised ZNFX1 functions as a dsRNA sensor to initiate antiviral responses through MAVS. *Nat. Cell Biol.* 21, 1346–1356. <https://doi.org/10.1038/s41556-019-0416-0>.
 48. Wang, X., Hennig, T., Whisnant, A.W., Erhard, F., Prusty, B.K., Friedel, C.C., Forouzmand, E., Hu, W., Erber, L., Chen, Y., et al. (2020). Herpes simplex virus blocks host transcription termination via the bimodal activities of ICP27. *Nat. Commun.* 11, 293. <https://doi.org/10.1038/s41467-019-14109-x>.
 49. Rutkowski, A.J., Erhard, F., L'Hernault, A., Bonfert, T., Schilhabel, M., Crump, C., Rosenstiel, P., Efstatiou, S., Zimmer, R., Friedel, C.C., and Dölen, L. (2015). Widespread disruption of host transcription termination in HSV-1 infection. *Nat. Commun.* 6, 7126. <https://doi.org/10.1038/ncomms8126>.
 50. Wang, X., Liu, L., Whisnant, A.W., Hennig, T., Djakovic, L., Haque, N., Bach, C., Sandri-Goldin, R.M., Erhard, F., Friedel, C.C., et al. (2021). Mechanism and consequences of herpes simplex virus 1-mediated regulation of host mRNA alternative polyadenylation. *PLoS Genet.* 17, e1009263. <https://doi.org/10.1371/journal.pgen.1009263>.

STAR★METHODS

KEY RESOURCES TABLE

REAGENT or RESOURCE	SOURCE	IDENTIFIER
Antibodies		
Rabbit polyclonal anti-CPSF6	Novus Biologicals	Cat# NBP1-85676; RRID: AB_11004635
anti- β -actin	FUDE Biologicals	Cat# FD0060; RRID: AB_2923199
Mouse polyclonal anti-CPSF5	Proteintech	Cat# 10322-1-AP; RRID: AB_2251496
Rabbit polyclonal anti-CPSF7	Proteintech	Cat# 55195-1-AP; RRID: AB_10858797
Recombinant Anti-SYVN1/HRD1 antibody	abcam	Cat# ab170901; RRID: AB_2833021
Rabbit polyclonal anti-HRD1	Novus	Cat# NB100-2526; RRID: AB_608700
Ubiquitin (P37) Antibody	Cell Signaling Technology	Cat# 58395S; RRID: AB_3075532
Ubiquitin Antibody	Santa Cruz Biotechnology	Cat# sc-271289; RRID: AB_10611436
Rabbit Anti-HA Tag RB0411 Polyclonal Antibody	abcepta	Cat# AP1012a; RRID: AB_352510
Mouse monoclonal anti-Myc	Sigma	Cat# M4439; RRID: AB_439694
Monoclonal ANTI-FLAG® M2 antibody produced in mouse	Sigma	Cat# F1804; RRID: AB_262044
K48-linkage Specific Polyubiquitin (D9D5) Rabbit mAb	Cell Signaling Technology	Cat# 8081; RRID: AB_10859893
K63-linkage Specific Polyubiquitin (D7A11) Rabbit mAb	Cell Signaling Technology	Cat# 5621; RRID: AB_10827985
Anti-rabbit IgG	Cell Signaling Technology	Cat# 7074; RRID: AB_2099233
Anti-mouse IgG HRP-linked Antibody	Cell Signaling Technology	Cat# 7076; RRID: AB_330924
Goat anti-Rabbit IgG (H + L) CrossAdsorbed Secondary Antibody, Alexa Fluor™ 568	Invitrogen	Cat# A-11011; RRID: AB_143157
Goat anti-rabbit IgG (H + L) CrossAdsorbed Secondary Antibody, Alexa Fluor™ 488	Invitrogen	Cat# A-11008; RRID: AB_143165
anti-Lamin B1	Cell Signaling Technology	Cat# 13435; RRID: AB_2737428
MyD88 (D80F5) Rabbit mAb	Cell Signaling Technology	Cat# 4283; RRID: AB_10547882
MAVS (D5A9E) Rabbit mAb	Cell Signaling Technology	Cat# 24930; RRID: AB_2798889
RIG-I (D14G6) Rabbit mAb	Cell Signaling Technology	Cat# 3743; RRID: AB_2269233
TRIF Antibody	Cell Signaling Technology	Cat# 4596; RRID: AB_2256555
MDA5 Recombinant Rabbit Monoclonal Antibody (33H12L34)	Thermo Fisher Scientific	Cat# 700360; RRID: AB_2532316

(Continued on next page)

Continued

REAGENT or RESOURCE	SOURCE	IDENTIFIER
IRF-3 (D83B9) Rabbit mAb	Cell Signaling Technology	Cat# 4302; RRID: AB_1904036
TBK1/NAK (D1B4) XP(tm) Rabbit mAb	Cell Signaling Technology	Cat# 3504; RRID: AB_2255663
cGAS Polyclonal antibody	proteintech	Cat# 26416-1-AP; RRID: AB_2880507
Recombinant Anti-ZNFX1 antibody	abcam	Cat# ab179452; RRID: AB_3073968
Mouse Anti-VSV Glycoprotein Monoclonal Antibody	Sigma	Cat# V5507; RRID: AB_261877
Bacterial and virus strains		
VSV	Our laboratory	N/A
VSV-eGFP	Our laboratory	N/A
HSV-1	Our laboratory	N/A
Sev	Our laboratory	N/A
EMCV	Our laboratory	N/A
Chemicals, peptides, and recombinant proteins		
Opti-RPMI-1640	Thermo	Cat# C11875500BT
Opti-DMEM	Thermo	Cat# C11995500BT
FBS Fetal Bovine Serum, Qualified	FBS Fetal Bovine Serum, Qualified	Cat# 10091148
DEPC H ₂ O	Invitrogen	Cat# AM9922
Puromycin	Gibco	Cat# A1113803
RIPA Lysis Buffer	Beyotime Biotechnology	Cat# P0013B
5× DualColor protein loading buffer	FUDE Biologicals	Cat# FD002
T4 DNA ligase	New England BioLabs	Cat# M0202
PMA	Solarbio	Cat# P6741-5mg
MG132	MCE	Cat# HY-13259-10mg
Poly(I:C)(LMW)	Invitrogen	Cat# tirl-picw
Poly(dA:dT)naked	Invitrogen	Cat# tirl-patn
5ppp-hpRNA	Invitrogen	Cat# tirl-hprna
LS-102	MCE	Cat# HY-135844-5mg
RNAiMax	Thermo Fisher Scientific	Cat# 13778150
Immobilon Western	Millipore	Cat# WBKLS0500
Chemiluminescent HRP Substrate		
DAPI Staining Solution	Beyotime Biotechnology	Cat# C1005
TRIZOL	Sigma	Cat# T9424
Critical commercial assays		
Endo-free Plasmid Mini Kit II	Omega	Cat# D6950
Gel Extraction Kit	Omega	Cat# D2500
Deposited data		
IVT-SAPAS raw sequence data	This paper	NCBI GEO: GSE284508 https://www.ncbi.nlm.nih.gov/geo/query/acc.cgi CNCB: PRJCA026962 https://ngdc.cncb.ac.cn/gsa/browse/CRA021324

(Continued on next page)

Continued

REAGENT or RESOURCE	SOURCE	IDENTIFIER
Original Western blotting images and qPCR data	This paper	
Experimental models: Cell lines		
Human: THP-1	Our laboratory	N/A
Human: HEK293T	ATCC	Cat# CRL-3519
Mouse: L929	ATCC	Cat# CCL-1
Human: A549	ATCC	Cat# CCL-185
Experimental models: Organisms/strains		
DH5 α	Tsingke Biotechnology	Cat# TSV-A07
Oligonucleotides		
See Table S3 for primers used in this study	Tsingke Biotechnology	N/A
Recombinant DNA		
pLKO.1 and derivatives (plasmids)	This paper	N/A
pCMV and derivatives (plasmids)	This paper	N/A
HA-WT	This paper	N/A
HA-K6	This paper	N/A
HA-K11	This paper	N/A
HA-K27	This paper	N/A
HA-K29	This paper	N/A
HA-K33	This paper	N/A
HA-K48	This paper	N/A
HA-K63	This paper	N/A
Experimental models: Organisms/strains		
C57BL/6J	GuangDong medical laboratory animal center	N/A
Software and algorithms		
ImageJ	NIH	https://imagej.nih.gov/ij/
GraphPad Prism 8	GraphPad Prism Software	http://www.graphpad.com/scientificsoftware/prism/
R v4.1.2/v3.4.1	R Project	https://www.r-project.org/

EXPERIMENTAL MODEL AND STUDY PARTICIPANT DETAILS

Animals

C57BL/6 mice, 6–8 weeks old, male and female mice were obtained from the Guangdong Medical Animal Research Center, and housed in a specific pathogen-free environment with a 12-h light/dark cycle and a temperature of 20°C–25°C. All experimental procedures involving mice were approved by the Institutional Animal Care and Use Committee (IACUC) of Sun Yat-sen University, Guangzhou, China.

Cell culture

Human cells of THP-1, A549 and HEK293T and mouse L929 cells were acquired from ATCC and maintained in our laboratory. THP-1 and L929 cells were maintained in RPMI-1640 (Gibco) supplemented with 10% fetal bovine serum (FBS; ExCell Bio) at 37°C with 5% CO₂ incubation. A549 and HEK293T cells were maintained in DMEM (Gibco) supplemented with 10% FBS (ExCell Bio) at 37°C with 5% CO₂ incubation. The cells have been identified with STR and tested for mycoplasma contamination.

Mouse bone marrow-derived macrophages (BMDMs) and peritoneal-derived macrophages (PMs) were isolated from 6 to 8 weeks old male and female C57BL/6J mice (Guangdong Medical Experimental Center). After overnight cultivation of BMDM at 37°C in 5% CO₂, the cell supernatant was collected and the cell pellet was obtained by centrifugation. The cells were cultured in DMEM medium supplemented with 1% penicillin-streptomycin, 10% FBS, 50 ng/ml macrophage colony stimulating factor (PeproTech) and cultured with 50 ng/ml macrophage colony stimulating factor for 8 days. BMDMs and PMs were both cultured in DMEM (Gibco) supplemented with 10% FBS (Gibco) and 1% penicillin-streptomycin (Gibco).

METHOD DETAILS

RNA extraction and qRT-PCR

Total RNA was extracted with TRizol reagent (Invitrogen). Evo M-MLV RT kit (Accurate Biology) was used to synthesize cDNA. The qRT-PCR was performed on a LightCycler 480 (Roche) using SYBR Green pro-tag mix (Accurate Biology). The data for each sample are normalized to the expression of actin mRNA. Relative gene mRNA expression was assessed by $2^{-\Delta\Delta Ct}$. Primers are listed in Table S3.

Virus infection

Vesicular stomatitis virus (VSV), VSV-eGFP, herpes simplex virus 1 (HSV-1), Sendai virus (SeV) and Encephalomyocarditis virus (EMCV) were preserved in our laboratory. Cells were infected with the virus at the indicated MOI in serum-free DMEM or RPMI-1640 for 1 h, washed with 1× PBS and incubated with fresh complete medium for duration time indicated in the figures.

Analogue stimulation

THP-1 cells were treated with PMA (50 ng/mL) for 48h and then replaced with RPMI-1640 complete medium and continued to be cultured for 24h. Cells were stimulated with 1 µg/mL poly(dA:dT), poly(I:C), and 5'ppp-hpRNA delivered by jetPRIME Reagent (Polyplus). Cells were harvested after 0, 2, 4, 8, 12, 24h of stimulation.

Proteasome and autophagy inhibitor treatment

THP-1 cells were treated with PMA (50 ng/mL) for 48h and then replaced with RPMI-1640 complete medium and continued to be cultured for 24h. The cells were simultaneously treated with proteasome inhibitor MG132 (10 µM) or autophagy inhibitor 3-methyladenine (3-MA) (5 mM) and baflomycin A1 (Baf-A1) (10 nM) for 8h.

siRNA transfection

Small RNA was transfected by using Lipofectamine RNAiMAX Reagent (Invitrogen) following the manufacturer's instructions. siRNAs were from Tsingke Biotech. The siRNA sequences used to achieve higher levels of silencing are shown in Table S4.

Plasmid transfection

Plasmid transfection was performed by Transporter 5 Transfection Reagent (Polysciences) following the manufacturer's instructions. HEK293T cells were inoculated into a six-well plate 24h before transfection and the cells were harvested 48h after transfection with plasmids.

Stable knockdown or overexpression cell lines

DNA fragments of wildtype and mutants of CPSF6 (K161R, K185R, K161R/K185R) were amplified with specific primers, and lentiviral vectors of PCDH-Puro-Myc-CPSF6, PCDH-Puro-Myc-CPSF6-K161R, PCDH-Puro-Myc-CPSF6-K185R, PCDH-Puro-Myc-CPSF6-K161R/K185R were constructed. All PCR primers are listed in Table S3. The online shRNA design tool (<http://rnaidesigner.thermofisher.com/>) was used to design the shRNA sequence targeting human CPSF6, SYVN1 and MAVS. The designed shRNAs are shown in Table S4.

Then Lentiviruses were produced by packaging HEK293T cells with the plasmids and the supernatants were collected at 48 and 72h after transfection. The virus was filtered through a 0.45 µm filter and the L929 cells were then infected with the appropriate amount of virus. Finally, the cells were screened and cultured in medium containing puromycin (1 µg/mL) for 1–2 weeks.

THP-1 cells or A549 cells were infected with the pLKO.1 lentiviral vector carrying a target gene sequence or a scrambled shRNA. After 24h of culture, cells were selected by the addition of puromycin (2 µg/mL) to the medium.

Western blot

The cells were washed three times with 1× PBS and then lysed in cold lysis buffer (50 mM Tris HCl pH 7.4, 150 mM NaCl, 0.1% SDS, 1% NP-40, 1mM PMSF, 1× Protein Inhibitor Cocktail (Roche)) at 4°C for 30 min. Cell debris was removed by centrifugation at 12000g for 15 min. Protein concentrations were determined using the BCA assay kit (Thermo Scientific). The supernatant of the lysate was then in 5 × DualColor protein loading buffer (FD002, FUDE, Hangzhou) for 10 min. Proteins were separated on 10% SDS-polyacrylamide gels. The gel was then transferred to nitrocellulose membranes. It was blocked for 1h at ambient temperature in blocking solution (1× PBST containing 5% BSA). The membrane was then incubated with primary antibodies overnight at 4°C. The membrane was then washed with 1× PBST and incubated with the appropriate secondary antibody for 1h at room temperature. The signal intensity was determined using the Tanon 5200s chemiluminescence imaging system (Tanon). Images were cropped for presentation. Marker 10-180kD (MIK).

Phos-tag SDS PAGE and western blotting

The cells were washed three times with 1× PBS and then lysed in cold lysis buffer (50 mM Tris HCl pH 7.4, 150 mM NaCl, 0.1% SDS, 1% NP-40, 1mM PMSF, 1× Protein Inhibitor Cocktail (Roche)) or lysis buffer containing 1 × phosphatase inhibitors PhosSTOP (Roche) at 4°C for 30 min. Cell debris was removed by centrifugation at 12000g for 15 min. Protein concentrations were determined

using the BCA assay kit (Thermo Scientific). The supernatant of the lysate was then in 5 × DualColor protein loading buffer (FD002, FUDE, Hangzhou) for 10 min. Proteins were separated on 6% SDS-polyacrylamide gels with 50 mM Phos-tag acrylamide (FUJIFILM Wako Chemicals, USA) and 0.1 mM Mn²⁺.

The gel was then transferred to nitrocellulose membranes. It was blocked for 1 h at ambient temperature in blocking solution (1 × PBST containing 5% BSA). The membrane was then incubated with primary antibodies overnight at 4°C. After electrophoresis, the gel containing Phos tag was washed three times in a transfer buffer (1 × Western Transfer Buffer: 0.025 M Tris, 0.20 M Glycine, 20% methanol) containing 10 mM EDTA for 15 min each time. Then place it in a buffer solution without EDTA for 15 min. The following steps are consistent with regular Western blot.

Immunoprecipitation analysis

The cells were transfected with plasmid into HEK293T cells and the cells were collected after 48 h. Cells were lysed in IP lysis buffer (pH = 7.4, 25 mM Tris-HCl, 150 mM NaCl, 1% NP40, 1 mM EDTA, 5% glycerol, 1 mM PMSF (Sigma), 1 × Protease inhibitor cocktail (Roche), and 1 mg/mL RNase A (Sigma)) at 4°C for 30 min. The cell lysate was then centrifuged at 12000g for 15 min to remove cell debris. Protein concentrations of the extracts were measured with BCA assay kit (Thermo Fisher). The supernatant was incubated with the appropriate antibody for 2 h at room temperature. Protein G beads (Invitrogen, 10003D) were prewashed (50 mM Tris-HCl pH 7.4, 150 mM NaCl) and incubated with supernatant for 1 h. The beads were then washed three times with wash buffer and the protein complexes were eluted by heating for 10 min in 1 × protein loading buffer for the next western blotting analysis. Equal amounts of proteins were loaded for SDS-PAGE, transferred to nitrocellulose or PVDF (Polyvinylidene Fluoride) membranes and then blotted with the indicated antibodies. PVDF membrane for detection of ubiquitination modification.

Immunofluorescence

Cells were grown on confocal culture dishes (NEST, 801002) and infected with VSV-eGFP at different time points. The cells are then washed with 1 × PBS and fixed with 4% paraformaldehyde for 10 min at RT. After three washes with 1 × PBS for 5 min each, the cells were permeabilized with 0.25% Triton X-100 in 1 × PBS for 10 min at RT. The cells were blocked with 5% BSA for 1 h at RT and incubated with primary antibodies after three washes with 1 × PBS for 5 min each. The primary antibodies were coupled with Alexa Fluor 488 or Alexa Fluor 568 after three washes with 1 × PBST. DAPI (Beyotime Biotechnology, 1:500) was used for DNA staining after three washes with 1 × PBS for 5 min each. Finally, the cells were washed again with 1 × PBS and images were captured on a Leica TCS SP8 STED microscope in confocal mode using a 1003 oil immersion/1.4 N.A. or 633 oil immersion/1.4 N.A. objective (Leica TCS SP8 STED). Data were analyzed using ImageJ software.

Antibodies

The antibodies used in western blotting, Co-IP, and immunofluorescence are as follows: Myc-tag (Sigma, M4439), FLAG tag (Sigma, F1804), CPSF6 (Novus, NBP1-85676), SYVN1 (abcam, ab170901), SYVN1 (Novus, NB100-2526), CPSF5 (Proteintech, 66335-1-Ig), CPSF7 (Proteintech, 55195-1-AP), Ubiquitin (P37) Antibody (Cell Signaling Technology, 58395S), Ubiquitin Antibody (Santa Cruz Biotechnology, sc-271289), K48-linkage Specific Polyubiquitin (Cell Signaling Technology, 8081), K63-linkage Specific Polyubiquitin (Cell Signaling Technology, 5621T), anti-β-actin (FUDE Biologicals, FD0060), GAPDH (Proteintech, 60004-1-Ig), IgG-rabbit (Cell Signaling Technology, 2729S), HRP-linked-mouse (Cell Signaling Technology, 7076S), HRP-linked-rabbit (Cell Signaling Technology, 7074S), Alexa Fluor 568 labeled-rabbit (Invitrogen, A-11011), Alexa Fluor 488 labeled-mouse (Invitrogen, A-11001).

IVT-SAPAS library

THP-1 cells were treated with PMA for 48 h and cultured in RPMI-1640 complete medium for 24 h. Samples were collected by TRIZOL after treatment of the cells with VSV (MOI = 1) for 4, 8, 12 h. According to the previous report (Fu et al., 2015), total RNA was extracted, and APA sequencing was performed using IVT-SAPAS.

QUANTIFICATION AND STATISTICAL ANALYSIS

Sequencing reads of IVT-SAPAS were trimmed and filtered, mapped to the human genome (hg38), and the 3' UTR switch of each APA gene was analyzed as previously described (Fu et al., 2015).

The average fluorescence intensity of VSV-eGFP in cells was analyzed using “Measure RGB” in ImageJ, and one field of view with 100× magnification was randomly analyzed at different time points from three biological repeats. The grouped line plots were realized using the ggplot2 package in R.

The ratios of SYVN1 in the nucleus were analyzed with the IF image. “Split Channels” in ImageJ was used to split the RGB channels of the IF image. The nucleus in the blue channel and the whole cell in the red channel were selected with “Polygon Selection”, and then the total fluorescence intensity of SYVN1 in the nucleus, the whole cell in the red channel were measured, and then the proportions of SYVN1 in the nucleus to the whole cell were calculated. Violin plots were drawn using the ggpunr package for R. Two-way ANOVA was performed to test the interaction effect of virus infection and MAVS on the nucleus localization of SYVN1. T tests were performed to compare the difference of two groups as described in figure legends.